CHANGES IN MINING INDUCED SEISMICITY BEFORE AND AFTER THE CRANDALL CANYON MINE COLLAPSE

by

Tex Mitchel Kubacki

A thesis submitted to the faculty of
The University of Utah
in partial fulfillment of the requirements for the degree of

Master of Science

Department of Mining Engineering

The University of Utah

May 2014

The University of Utah Graduate School

STATEMENT OF THESIS APPROVAL

The thesis of **Tex Mitchel Kubacki**

has been approved by the following supervisory committee members:

M. K. McCarter	, Chair	**7 March 2014** Date Approved
Keith Koper	, Co-chair	**7 March 2014** Date Approved
Michael G. Nelson	, Member	**7 March 2014** Date Approved

and by **Michael G. Nelson** , Chair/Dean of

the Department/College/School of **Mining Engineering**

and by David B. Kieda, Dean of The Graduate School.

ABSTRACT

On August 6, 2007, the Crandall Canyon Mine in central Utah experienced a major collapse that was recorded as an M_w 4.1 seismic event. Application of waveform cross-correlation detection techniques to data recorded at permanent seismic stations located within ~30 km of the mine has resulted in the discovery of 1,494 previously unknown microseismic events related to the collapse. These events occurred between July 26, 2007, and August 19, 2007, and were detected with a magnitude threshold of completeness of 0.0, about 1.6 magnitude units smaller than the threshold associated with conventional techniques. Relative locations for the events were determined using a double-difference approach that incorporated absolute and differential arrival times. Absolute locations were determined using ground-truth reported in mine logbooks. Lineations apparent in the newly detected events have strikes similar to those of known vertical joints in the mine region, which may have played a role in the collapse. Prior to the collapse, seismicity occurred mostly in close proximity to active mining, though several distinct seismogenic hotspots within the mine were also apparent. In the 48 hours before the collapse, changes in b-value and event locations were observed. The collapse appears to have occurred when the migrating seismicity associated with direct mining activity intersected one of the areas identified as a seismic hotspot. Following the collapse, b-values decreased and seismicity clustered farther to the east.

“Geologic time includes now.”

-Gerry Roach

TABLE OF CONTENTS

LIST OF FIGURES

ACKNOWLEDGEMENTS

Thank you to Drs. Kim McCarter, Keith Koper, and Kristine Pankow for all of their immeasurable assistance and support on this project. Thank you also to Michael Nelson, Meagan Boltz, Mark Hale, Paul Roberson, Katherine Whidden, Jessica Wempen, Derrick Chambers, Jared Stein, Jim Pechmann, Walter Arabasz, William Pariseau, Jamie Farrell, Pam Hofmann, and Bill Blycker for their technical support. Further recognition goes to Sam Margulies, Carrie Welker, Mary Glenn Mellor, Chloë Simons, Aaron Young, Julie Bare, Manas Pathak, Zoro The Cat, and Rachel Anderson for all of their guidance along the way. This research was made possible through funding and support from NIOSH grant #200-2011-39614 and the State of Utah. The views and conclusions contained in this document are those of the author and should not be interpreted as representing the opinions or policies of NIOSH or other sponsors of this research.

CHAPTER 1

INTRODUCTION

On August 6, 2007, the Crandall Canyon Mine (CCM) in Emery County, Utah, experienced a catastrophic collapse that trapped six mineworkers approximately 600 m underground. The workers had been mining coal from a room-and-pillar section of the mine as part of a pillar recovery project begun in late 2006. Attempts to reopen a collapsed mine entry to reach the suspected location of the trapped mineworkers resulted in a violent burst of coal from the side of the entry, fatally injuring three rescue-workers on August 16, 2007, and ending any further rescue attempts (MSHA 2007).

The CCM collapse was well recorded by permanent stations of the regional seismic network operated by the University of Utah Seismograph Stations (UUSS). Analysis of the seismic data yielded a magnitude estimate of M_L 3.9 (M_C 4.5), epicenter of 39.4675° N 111.2248° W, depth of 0.5 km, and origin time of 8:48:39.87 UTC (Pechmann et al. 2008). Full moment tensor inversion of regional distance waveforms resulted in a moment magnitude of M_w 4.1 and revealed that the event had a significant (76%) vertical collapse component (Dreger et al. 2008), inconsistent with the double-couple nature of tectonic earthquakes and consistent with mathematical models of a closing crack.

Systematic full moment tensor inversion of 44 seismic events that occurred in the Utah region during the period of 1998–2011 reinforced the dominant collapse nature of

the August 6, 2007, seismic event (Whidden and Pankow 2012). Although significantly isotropic, the observation of Love waves suggests there was a small double-couple component to the CCM event (Ford et al. 2008; Dreger et al. 2008). A pure collapse model is also inconsistent with satellite-based measurements of subsidence, which require a minor component of sympathetic normal faulting above the collapse area (Plattner et al. 2010; Lu and Wicks 2010).

Shortly after the collapse, UUSS deployed five temporary seismic stations within 7 km of the epicenter to help detect and locate aftershocks. These stations are shown in Figure 1.1. Data from these stations were integrated into the permanent UUSS network and reduced the detection threshold in the area from M_L 1.6 to M_L 1.2. For 1 month following the collapse, UUSS located 37 seismic events that were within 3 km of the epicenter. In the absence of active mining, these events are assumed to be causally related to the collapse and are not the manifestation of normal mining-induced seismicity as detailed by Pankow et al. (2008). Other mine collapses have likewise produced robust aftershock sequences (Phillips et al. 1999; Trifu and Sumila 2010).

Examination of logbooks kept by the rescue workers showed that many of the felt seismic events occurred in the 7 days following the collapse, before the temporary network went online, but were too small ($< M_L$ 1.6) to trigger the UUSS detection system. Ten of these small events, ranging in magnitude from M_C 0.4 to M_C 1.6, were identified through detailed inspection of continuous seismic waveforms (Kubacki et al. 2012). The newly identified events were added to the original catalog (Pechmann et al. 2008), and all events were relocated using a double-difference inversion method (Waldhauser and Ellsworth 2000). Location errors were reduced by 24% when compared

with reported ground-truth locations (Kubacki et al. 2012). During this process, numerous arrivals from additional undetected aftershocks were apparent in the seismic record, and it was hypothesized that many more microseismic events may have occurred in the weeks leading up to the collapse than had been detected by standard UUSS analysis procedures.

In this study, waveform correlation techniques are applied to data from permanent UUSS stations in the CCM area to detect and locate as many aftershocks as possible and to better characterize the precollapse seismicity in the mine region. Waveform-based cross-correlation detection techniques have been shown to perform better than short-term average/long-term average detection algorithms in cases where repeating seismic events occur in tight spatial clusters. Many cross-correlation detection studies have demonstrated greater than one magnitude unit reduction in detection threshold (Gibbons and Ringdal 2006; Harris 2006; Harris and Paik 2006; Schaff 2010). Furthermore, highly accurate relative wave arrival times can be determined through sliding-window cross-correlation comparisons between detected events (VanDecar and Crosson 1990; Schaff and Waldhauser 2005). These “lag-times” can be used to invert for precise relative locations (Shearer 1997; Rubin et al. 1999; Schaff et al. 2004, Hauksson and Shearer 2005; Waldhasuer and Schaff 2008).

The resulting seismicity catalog for the CCM area is analyzed to better understand the sequence of collapse. Differences in precollapse and postcollapse seismicity, as observed through spatial clustering patterns, frequency-magnitude relations, and aftershock decay rates, give insight into the mechanics of the collapse as well as the changing states of stress within the mine. The observations from the temporary stations are further used to justify detector thresholds and validate the new catalog.

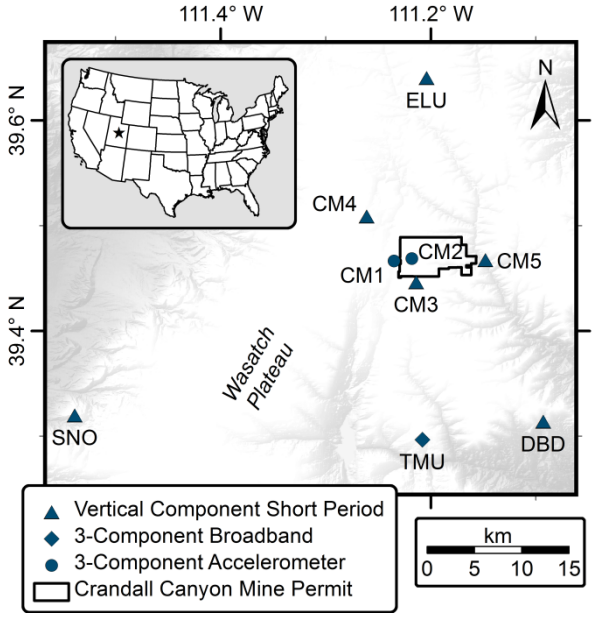

Figure 1.1 Mine permit and station geometry

CHAPTER 2

SEISMIC DATA

The CCM is located on the northwestern edge of the Wasatch Plateau and Book Cliffs coal-mining region in Emery County, Utah (Figure 1.1). This area is roughly 150 km southeast of Salt Lake City, Utah, and has been home to numerous coal mines since 1874 (Doelling 1972). As of 2005, there were at least 13 active coal mines in the region. Of those, eight were engaged in longwall mining, and five practiced methods of pillar extraction (Pankow et al. 2008). The CCM began in 1939 as a room-and-pillar operation in the Hiawatha coal seam, one of the most economically important beds in the region (MSHA 2007; Doelling 1972). In 1994, the CCM began longwall mining, but returned to pillar extraction in 2005 (MSHA 2007). A room-and-pillar section of the CCM known as "Main West" was targeted for pillar recovery beginning in late 2006. The area directly north of Main West had been previously mined out via longwall in 1999, leaving a 137-m-thick barrier pillar known as "North Barrier." Extraction proceeded in North Barrier of Main West until damage from a M_L 1.8 seismic event on March 10, 2007, caused miners to abandon the North Barrier in favor of the southern section ("South Barrier") of Main West (Pechmann et al. 2008).

The UUSS regional seismic network has been monitoring mining-induced seismicity in Utah since 1978. Mining-induced seismicity (MIS) is closely related in time and location to underground coal extraction and is prevalent in the active coal mines of

Utah's Wasatch Plateau and Book Cliffs regions (Arabasz et al. 1997; Arabasz and Pechmann 2001; Pankow et al. 2008; Boltz et al. 2014). Between 2004 and 2007, UUSS located an average of 1,444 mining-induced events per year, with magnitudes ranging from M_L -0.2 to M_L 3.9, though mostly below M_L 3.0 (Pankow et al. 2008). MIS occurs in mining regions around the world, and comprehensive reviews are given by Hasegawa et al. (1989) and Gibowicz (2009).

At the time of the August 6, 2007 collapse, there were five seismograph stations within 40 km of the CCM (Figure 1.1). The closest UUSS station, TMU, was a three-component broadband seismometer with 100-Hz sampling. The other three nearby UUSS stations (DBD, ELU, and SNO) were vertical component, short-period seismometers with 100-Hz sampling. A fifth station, a three-component broadband element of the Earth Scope Transportable Array (TA) with station code P16A, was located 40 km to the WNW of the epicenter and was sampled at 40 Hz. In addition to these stations, five temporary seismometers were deployed within five days following the collapse. These were designated CM1, CM2, CM3, CM4, and CM5. The two stations closest to the collapse, CM1 and CM2, were three-component Applied MEMS accelerometers (Pechmann et al. 2008). They went online on August 8, both recording at 100 Hz, with the continuous digital data being archived. Continuous data from analog stations CM3, CM4, and CM5 were not archived. For these analog stations, only waveform segments from triggered events were saved. The temporary stations remained online until October 3, 2007.

Using routine UUSS procedures (Burlacu et al. 2007) with all the regional data, 55 seismic events were located in the vicinity of CCM during the month of August 2007.

Combining these 55 events with 144 other events occurring within a 3-km radius of the mine between August 2, 2005 and July 31, 2007, Pechmann et al. (2008) relocated the CCM seismicity using the *hypoDD* double-difference inversion method (Waldhauser and Ellsworth 2000). The relative locations of these events were then anchored to the known ground-truth location of the fatal August 16 rib-burst. These studies greatly helped to delineate the collapse sequence. For instance, the studies indicate that most aftershocks occurred along the eastern and western edges of the collapse zone, presumably where postcollapse stresses had increased. This migration of seismicity is similar to the tendency for well-located aftershocks of large earthquakes to cluster around patches of high coseismic slip (Ide et al. 2011; Hayes et al. 2013). A higher-resolution catalog of seismicity was needed, however, to determine the fine-scale structure of the aftershocks, confirm the apparent spatial gaps, better characterize the precollapse seismicity, and quantify any spatial or temporal changes in the seismicity in the lead-up to the collapse.

CHAPTER 3

METHODS

3.1 Correlation Based Detection of Seismicity

Waveforms from each of the original 55 seismic events located in the CCM area during August 2007 were used as templates for sliding-window cross-correlation against continuous data from UUSS stations TMU, ELU, DBD, and SNO, for the dates of July 26 through August 19, 2007. All initial detections were made at the closest station, TMU. Stations ELU, DBD, and SNO were used for detection verification and for calculating magnitudes, locations, and origin times of the newly detected events. Initial work showed that TA station P16A provided inferior quality detections, possibly because of its relatively larger distance (~40 km) from the collapse and relatively low Q path across the transition zone between the Colorado Plateau and Basin and Range physiographic provinces. It is unlikely that any station located farther from CCM (> 40 km away) would provide data useful for cross-correlation detection.

The data from the four usable stations were bandpass-filtered between 0.5 and 5.0 Hz before processing. This filter yielded acceptable signal-to-noise ratios after cross-correlations and was selected after an examination of several longer and shorter bandpass windows. A 15-second window was selected for each template event used for cross-correlation. Each 15-second window began five seconds after the origin time of the event and contained both P- and S-wave arrivals. Three of these template waveforms recorded

at station TMU are presented in Figure 3.1. Template #1 occurred on August 3 in close proximity to active mining. Template #32 occurred on August 16 to the east of the collapse. Template #34 corresponds to the August 16 event, which fatally injured three rescue-workers. The normalized cross-correlation coefficient, *cc*, was computed in the time domain, varying from –1 for a data segment perfectly out of phase with the template, to +1 for a data segment that is identical to the template event (autocorrelation). At TMU, the only usable three-component station, the three components of each template were concatenated and cross-correlated as one with the three concatenated components of each data segment (Yang et al. 2009). Figure 3.2 shows several hours of cross-correlation values around the time of the August 6 collapse for station TMU, using an M_L 1.5 template event. Large spikes indicate probable event detections, and the difference in precollapse and postcollapse activity is striking.

Slight differences in location, source mechanism, noise content, and prevailing velocity structure between template events and detected events result in imperfect matches ($cc < 1$). In many cases, it is difficult to determine whether a *cc* spike at a particular time is the result of a true detection or simply the result of well-correlated noise. Where thousands of detections are concerned, it is unfeasible to manually examine each *cc* spike in order to reject all false positives. Therefore, it is necessary to select a *cc* threshold with the goal of reducing false positives to an acceptable level while, at the same time, minimizing the number of missed detections. Only segments of continuous waveform data correlating above this threshold are accepted as true detections.

To properly select a *cc* detection threshold to be used at TMU, a baseline *cc* distribution was established by cross-correlating a representative template event with 1

hour of random noise recorded during a period of no known seismic events and minimal mining activity. Because prior studies have found that such *cc* distributions can be sensitive to the details of the particular noise sample used (Rowe et al. 2012), the process was repeated by correlating five different hour-long segments of noise and six random templates for a total of 30 distinct sets. A sample histogram of the resulting *cc* values is presented in Figure 3.3. Because *cc* values are physically constrained to range from –1 to +1, a Gaussian distribution cannot appropriately model these values. It is necessary to either transform the values into a domain where Gaussian statistics are appropriate (VanDecar and Crosson 1990) or to model the values with a different type of distribution. Probability distribution fitting analysis by means of the Anderson-Darling test yielded a best-fitting beta distribution:

$$f\left(x,\alpha,\beta\right)=\frac{x^{\alpha-1}\left(1-x\right)^{\beta-1}}{\int_0^1 u^{\alpha-1}\left(1-u\right)^{\beta-1}\,du} \qquad \text{(EQ 3.1)}$$

where α and β are shape parameters equal to 328.04±124.03 (1σ). Because poorly-correlated events can result in large location errors, a conservative *cc* threshold of 0.5 was selected as a basis for detections at station TMU. Using the probability density function (PDF) determined above, a *cc* threshold of 0.5 corresponds to a false-alarm probability of $3.21\text{x}10^{-31}$, or fewer than one false alarm per million years of data correlated against a template at a sample rate of 100 Hz.

Since many of the 55 template events generate *cc* spikes above the detection threshold within several hundredths of a second of one another, k-means clustering (MacQueen 1967) was used to avoid double counting. In other words, it was desirable to

avoid counting multiple templates that detected the same event at slightly different times as well as sidelobes associated with a true detection being declared as additional detections. This process involved automatically partitioning the *cc* spikes into distinct groups for each hour analyzed. Each group of nearby spikes was considered to represent one distinct detection. For each detection, the template event that produced the highest *cc* spike was noted and used to estimate origin time, location, and magnitude. This resulted in 2,115 unique event detections.

Because all initial detections were made using only the closest station (TMU), stations DBD, ELU, and SNO could be used to further confirm their validity. This was done by comparing magnitude estimates made at the four stations. For the purpose of magnitude estimation, it was assumed that every detected event differs only from its associated template event in amplitude and noise content. This makes it possible to compute an amplitude scaling factor:

$$\alpha = \frac{v_{\text{template}} \cdot v_{\text{detected}}}{v_{\text{template}} \cdot v_{\text{template}}} \qquad \text{(EQ 3.2)}$$

where α is equal to the unnormalized cross-correlation coefficient divided by the inner product of the template event (Schaff 2010), and ν is the vector of the template or detected event. These amplitude scaling factors were computed at each of the four stations using the most highly correlated template and the waveforms recorded at the detection times. The magnitude of a detected event can be computed at any station using α and the known magnitude of the template event. A final magnitude estimate is computed by averaging the magnitudes computed at the four stations:

$$M_{detected} = \sum\left[M_{template} + \log(\alpha)\right]/4 \quad \text{(EQ 3.3)}$$

In cases where the closest correlation peak to the primary detection is negative at one or more stations (detection out of phase), the magnitude is not calculable and the detection is discarded. This reduced the number of prospective detections from 2,115 to 2,100.

A final empirical check on the validity of cross-correlation detection process is possible using data from the two temporary stations CM1 and CM2 that were deployed in the mine region. For the period of August 8 at 20:06:10 through August 19, the waveform data corresponding to each of the detections made at station TMU were visually examined at stations CM1 and CM2 for evidence of a seismic event. Each of the 203 detections made during this time period using the procedures described above was confirmed, for 0 false detections. An example validation for an M –1.0 event is presented in Figure 3.4. Panel "a" shows the best-correlated template event. Panel "b" shows this template (red) shifted in time to a highly-correlated section of waveform data (black). Panels "c" and "d" show the high signal-to-noise ratio waveforms of the event recorded at the temporary stations CM1 and CM2. Amplitude (y-axis) is proportional to ground velocity and is scaled differently for each panel.

In order to determine the number of missed events, the *cc* detection threshold was systematically reduced from 0.50 to 0.45, 0.40, 0.35, and 0.30, corresponding to nominal false alarm probabilities of 2.00×10^{-34}, 5.59×10^{-27}, 1.06×10^{-20}, and 1.87×10^{-15} using the best-fitting beta PDF. As expected, decreasing the detection threshold increases both the number of true detections and the number of false detections. The reduced detection thresholds result in 219, 260, 309, and 484 true detections and 0, 3, 16, and 118 false detections, respectively, for August 9–19. Interestingly, the actual numbers of false

detections observed using the CM1 and CM2 data as ground truth are several orders of magnitude larger than the false detection rates predicted by the beta PDF. This suggests that the PDF fitting procedure is heavily dominated by the mass of *cc* spikes closest to the mean and does not accurately model low-probability events in the tail. This further justifies the choice of an extremely conservative *cc* threshold.

3.2 Double-Difference Relocation of Seismicity

The double-difference algorithm *hypoDD* (Waldhauser and Ellsworth 2000) is used to invert for relative locations of the detected events. Each detected event is placed at a starting position coincident with the best-known location of its associated template event. Lag-times at each station are computed between each detected event and all other detected events associated with the same template. In effect, this process preclusters the catalog and allows only the most strongly connected events to influence the inversion. The effects of uncertainties and changes in the assumed one-dimensional velocity model are reduced through this preclustering process (Boltz et al. 2014).

The resolution of event locations is partly dependent on the precision of the initial detection times (Cheng et al. 2011). This precision can be improved by resampling the template and continuous waveform data at a rate higher than the nominal value. This was done using the weighted average slopes method (Wiggins 1976), thus increasing all relevant sampling rates to 1 kHz. Using the detection times determined at 100 Hz as starting points, cross-correlations were recomputed within a 0.02-second time window at the new sampling rate. A significant improvement in event locations was seen upon relocating using the newly determined lag times. This process was repeated at a sampling rate of 10 kHz in order to test the stability of the event locations. No significant

difference was seen between locations computed using 1 kHz and 10 kHz data, implying that 1 kHz is sufficient. Because locations computed using the 10 kHz data are theoretically more accurate, they are used throughout the rest of this discussion.

The lag-times computed during the detection process are assumed to represent S-wave lag times, despite the correlation templates containing both P and S waves. S waves are typically higher in amplitude and appear to be more closely correlated than P waves in all examined detections. Attempts to correlate using separate P- and S-wave time windows did not yield reliable locations for many of the smaller magnitude events, most of which do not have clearly identifiable P waves.

Although all 55 templates were used for detection purposes, the detected events correlating best with 23 lower quality templates from the original set of 55 were rejected for the purpose of calculating locations. These 23 templates were unable to be located within the study area of Main West, and the removal of their associated detections does not alter the patterns in seismicity presented here. This removal resulted in the elimination of 644 poorly-located detections from the catalog.

While epicentral locations are well constrained, the depths of the detected events are more difficult to determine. It is often difficult to determine precise depths for mining-induced seismic events (Boltz et al. 2014). This is especially true when the closest station is ~20 km away. For the double-difference inversions performed in this study, depths are initiated at 0.6 km, very close to mine-level. Attempts to further constrain the depths using 30 P-wave arrival times picked at station CM1 did not significantly alter the locations.

It is assumed that the spatial structures and patterns of seismicity resulting from

the double-difference location technique represent the manifestation of geologic or mechanical features related to the CCM collapse (Waldhauser and Ellsworth 2000). As such, clearly defined seismic features resulting from this study are analyzed using jack-knifed eigenvalue decompositions to determine planarity, linearity, strike, and dip where possible (Michelini and Bolt 1986; Spottiswoode and Milev 1998).

Once cross-correlation detections and locations were completed for the August collapse, the process was repeated to study the seismicity surrounding the March 10 event that forced the mineworkers to abandon the North Barrier. A cross-correlation threshold of 0.5 was used along with 15 known template events as detectors. The resulting sequence of seismicity offers a useful comparison to the primary collapse sequence.

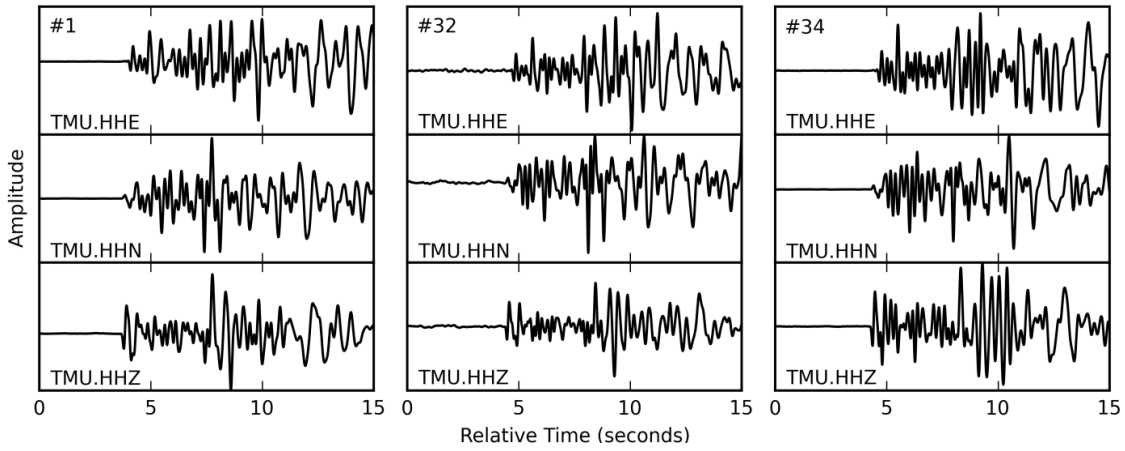

Figure 3.1. Seismograms of three sample template waveforms

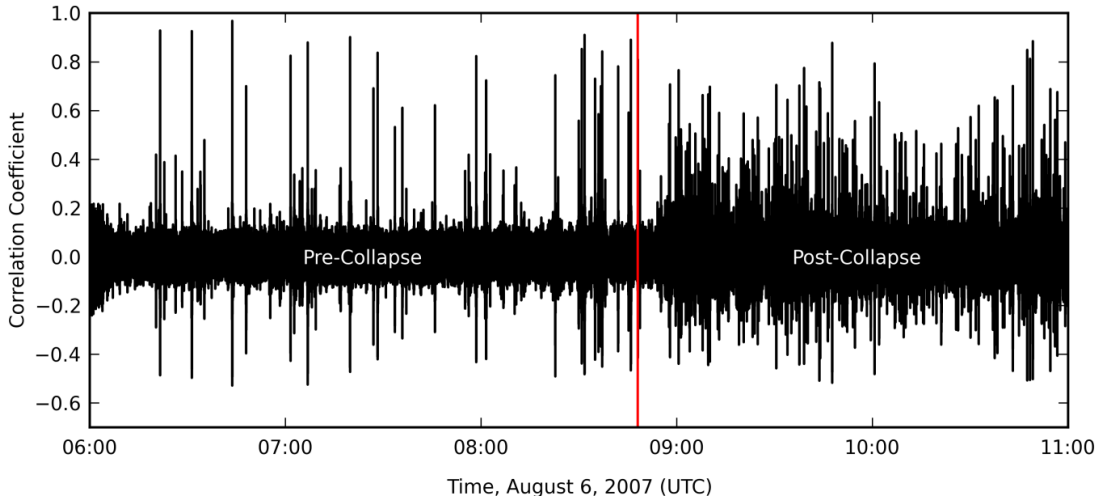

Figure 3.2. Cross-correlogram for several hours before and after the collapse

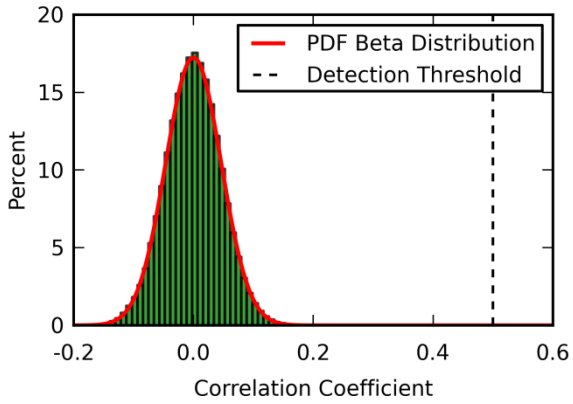

Figure 3.3. Beta distribution of *cc* values showing 0.5 threshold

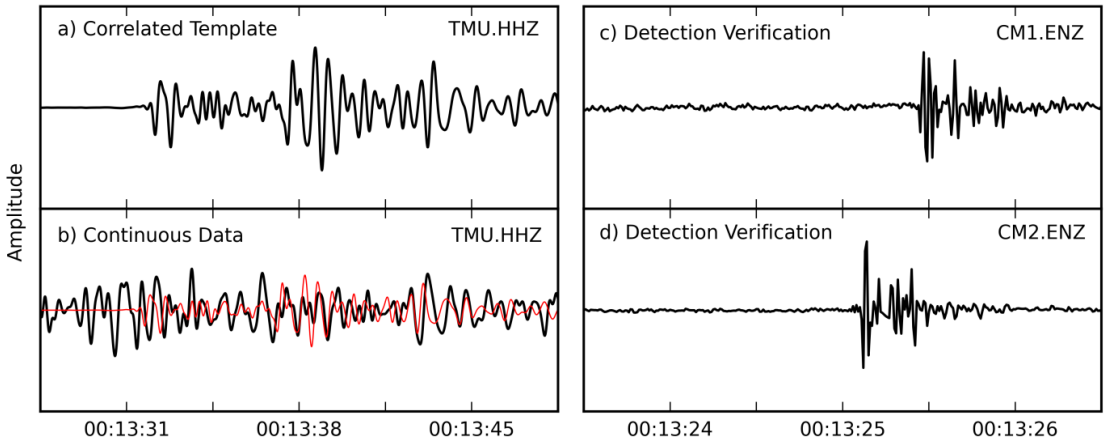

Figure 3.4. Detection of M –1.0 event at TMU validated at CM1 and CM2

CHAPTER 4

RESULTS AND DISCUSSION

4.1 Locations and Structures

A total of 1,494 seismic events were found to have occurred in close proximity to the collapse area between July 26 and August 19, 2007. The cross-correlation detection technique is based on the assumption that all detected events occur close in space and with similar source mechanisms to their associated template events. Double-difference inversion confirms that the final locations of the detected events remain in close proximity to their starting locations. Events detected by templates from the easternmost cluster tend to remain to the east of the collapsed area, while events to the west remain to the west. Plan views of these double-difference locations are included in Figure 4.1.

The top panel of Figure 4.1 displays all detected events dating from July 26, 2007 (the beginning of the study period), to 8:48 UTC, August 4, 2007 (48 hours before the mainshock). The area labeled "a" corresponds with a section of coal pillars actively being retreat-mined from west to east. The seismic events in this area progress likewise in time. The events located in the area labeled "b" are likely the result of abutment loading from the now-mined-out section. Eigenvalue analysis shows this event cluster to form a linear structure with strike of N30.59°E ± 1.45° (1σ). The events located in the area labeled "c" occurred in an inactive section of pillars. They appear to also form a linear structure with strike of N0.03°E ± 3.74°.

Linear and planar structures identified using the hypoDD algorithm suggest the existence of joints or faults (Waldhauser and Ellsworth 2000). Several fault zones run throughout the Wasatch Plateau. According to Doelling (1972), the most extensive of these is the Joes Valley Fault Zone. It runs for 121 km and is located approximately 12 km to the west of the CCM (Doelling 1972). Striking at roughly N15°E, the fault is nearly parallel to a major set of vertical joints spaced between 6 and 120 m and occurring in all known stratigraphic units throughout the region (Maleki Technologies, Inc. 2005). The two linear structures identified in the top panel of Figure 4.1 exhibit similar strikes to this well-documented set of vertical joints. The seismicity comprising the linear structures is possibly related to movement along these joints facilitated by the removal of the section of pillars between them. The events located in the area labeled "d" also occur in an inactive section of pillars. They coincide with the approximate future location of the fatal August 16 event.

The middle panel of Figure 4.1 displays all located events occurring no more than 48 hours prior to the mainshock. The events located in the area labeled "e" continue to progress from west to east in the direction and location of mining. The remaining cluster located to the northeast appears more diffuse. The collapse appears coincident in time with when mining progressed into close proximity of the diffuse cluster. The mainshock epicenter (Pechmann et al. 2008) is denoted by the blue star in the bottom panel of Figure 4.1.

The bottom panel of Figure 4.1 displays all detected events occurring between the time of the collapse and August 20, 2007 (the end of the study period). Seismicity no longer occurs in the location of the extracted pillars, but rather far to the east and west.

The events located in the area labeled “f” form a planar structure of seismicity on the eastern side of Main West. This structure formed quickly after the collapse and remained seismically active for several days. It is found to strike at N252.23°E ± 0.44° and to dip at 6.74° ± 0.04° to the north. It is more likely to be related to movement along bedding planes than to vertical joints. Because the bedding at CCM rarely dips greater than 3°, it is possible that the 6.74° calculated dip of the planar structure is slightly exaggerated by the relatively poor resolution in depth. In spite of this small discrepancy, there is considerable evidence to support that near-horizontal shearing occurred in the eastern section of Main West during the collapse. In addition to potential shearing components identified through moment tensor analysis (Ford et al. 2008), rescue workers reported observing pillars that had been shifted laterally in relation to the mine openings and to the presence of oxidized coal in the mine roof suggestive of shearing (MSHA 2007). The events located in the area labeled “g” coincide with the earlier events at “d” in the vicinity of August 16 fatal event.

The shifting of postcollapse seismicity to the area surrounding the collapse in the eastern portion of Main West is consistent with patterns observed in at least one prior study of mine collapse aftershocks (Phillips et al. 1999). Phillips et al. (1990) noted the apparent migration of overburden loading to surrounding, unmined areas of a Michigan copper mine following its induced collapse. At Crandall Canyon, however, there is a notable spatial gap in seismicity between the western event clusters (Figure 4.1, top panel, “a” and “c”) and the seismicity to the east (Figure 4.1, bottom panel, “f”). This may partly be explained by seismicity detected in the central portion of Main West related to the March 10 event and shown in Figure 4.2. Seismicity related to mining

during this time period may be responsible for weakening the already-compromised central roof of Main West and shifting loading to the easternmost pillars.

A total of 249 seismic events were found to have occurred in close proximity to the North Barrier of Main West between February 20 and March 18, 2007. Although there were much higher levels of seismicity surrounding the August collapse sequence, the two sequences do exhibit some similarity. Figure 4.3 shows a comparison of the average number of events per hour in 12-hour bins for both sequences. In both cases, the periodic increases and decreases preceding the mainshock may be related to breaks in mining and movement of equipment. The peak in seismicity of the March sequence, however, occurred approximately 7 hours prior to the mainshock, whereas the peak of the August sequence occurred immediately following the collapse. The August sequence exhibits a broader peak of sustained seismicity with a higher proportion of aftershocks occurring close in time. In contrast, levels of seismicity were already declining by the time the March mainshock occurred. In the days following the mainshock, seismic levels decreased rapidly in both cases, coincident with the cessation of mining.

4.2. Magnitude Threshold of Completeness

A magnitude threshold of completeness (M_{COMP}) for this sequence was determined using the software package ZMAP (Wiemer 2001). An M_{COMP} of 0.0 was computed for the detections related to the August collapse sequence. This was done after dividing the catalog of detections into the three periods represented in Figure 4.1. An M_{COMP} was selected for each one through visual inspection, and the largest of the three (0.0) is used for all further discussion of frequency-magnitude relations. An M_{COMP} of 0.0 represents a 1.6 magnitude unit reduction from the previous M_{COMP} of M_L 1.6 (Pechmann

et al. 2008), or a 40-fold improvement over standard processing techniques (Burlacu et al. 2007). In comparison, an M_{COMP} of 0.45 was computed for the detections related to the March 10 bump. Because the station array remained the same between the two time periods, the difference in M_{COMP} between the two sequences is likely due to the fact that only 12 detection templates were used in March, while 55 were used in August. The greater number of templates makes the detection of very small events more probable. It may also be possible that the March sequence simply did not include as many small-magnitude events as the August sequence did.

4.3. Frequency-Magnitude Relations

The frequency-magnitude relation of these two sequences can be linearly approximated on a logarithmic scale (Wiemer 2001). This type of b-value analysis can be used to compare the magnitudes observed in the two sequences of mining-induced seismicity to other, naturally-occurring or otherwise induced seismicity under various geologic conditions. The b-values reported here cannot be compared directly to those of declustered natural earthquake catalogs (Pechmann et al. 2008). This is because the seismicity considered here is comprised largely of repeating events, aftershocks, and foreshocks, which would all be removed during declustering. The August collapse sequence exhibits a b-value of 0.97 ± 0.04 (2σ), while the March bump sequence exhibits an overall b-value of 0.89 ± 0.05. The difference in b-values indicates a higher proportion of larger-magnitude events related to the August collapse and a higher proportion of smaller-magnitude events related to the March bump.

Time-variant b-values can be used as a way to gauge differential stresses. Prior studies of seismicity at CCM indicate a 50% decrease in b-value from the time before the

August collapse to the time after the August collapse (Pechmann et al. 2008). This trend holds with the addition of the newly detected events. A b-value of 1.23 ± 0.10 was computed for the events ranging from July 26 to 8:48 UTC on August 4 (Figure 4.1, top panel). A b-value of 1.12 ± 0.10 was computed for the events occurring within 48 hours prior to the mainshock (Figure 4.1, middle panel), representing a 8.9% reduction. A smaller b-value of 0.92 ± 0.05 was computed for the events occurring between the time of the collapse and August 20, 2007 (Figure 4.1, bottom panel). A frequency-magnitude plot comparing the first sequence (b = 1.29) and the last sequence (b = 0.87) is included as Figure 4.4. According to Pechmann et al. (2008), this decrease in b-value is either related to an increase in differential stress or to the migration of seismicity to the eastern portion of Main West where the local stress fields may differ. For comparison, the seismicity observed leading up to seaside chalk cliff collapses in western France also indicates a continuous decrease in b-value prior to the mainshock (Amitrano et al. 2005). This decrease is considered to be a possible precursory pattern to brittle failure. Because the events occurring in the 48 hours prior to the collapse remained localized to the western portion of the working section, the first change in b-value is likely related to a change in differential stress.

4.4. Temporal Decay of Aftershocks

The p-value statistic represents an exponential aftershock decay rate as defined by the Modified Omori's law (Utsu 1961):

$$N(t) = \frac{k}{(t+c)^p} \qquad \text{(EQ 4.1)}$$

where N(t) is the number of aftershocks per day, and c is the number of events per day at t = 1 – c days. This relation has been demonstrated to model aftershock decay rates observed for both naturally-occurring and mining-induced sequences of seismicity (Vallejos and McKinnon 2010). A p-value of 1.11 ± 0.06 (2σ) was computed for this catalog using ZMAP (Wiemer 2001). According to Vallejos and McKinnon (2010), the median p-value for 163 mining-induced seismicity sequences observed in four Canadian hard-rock mines was found to be 1.1, indicating close agreement. A prior study of seismicity at CCM found a p-value of 0.8 ± 0.3 using only 15 events with $M_C > 1.6$. The addition of newly detected events yields a p-value significantly higher than those computed for naturally-occurring earthquake sequences in Utah. According to Arabasz and Hill (1994), the average p-value for 11 earthquake sequences following $M_C > 4.5$ events between 1975 and 1992 was found to be 0.80 ± 0.13. Therefore, the aftershock sequence observed at CCM decays at a rate 28% higher than natural aftershock sequences observed under similar geologic conditions.

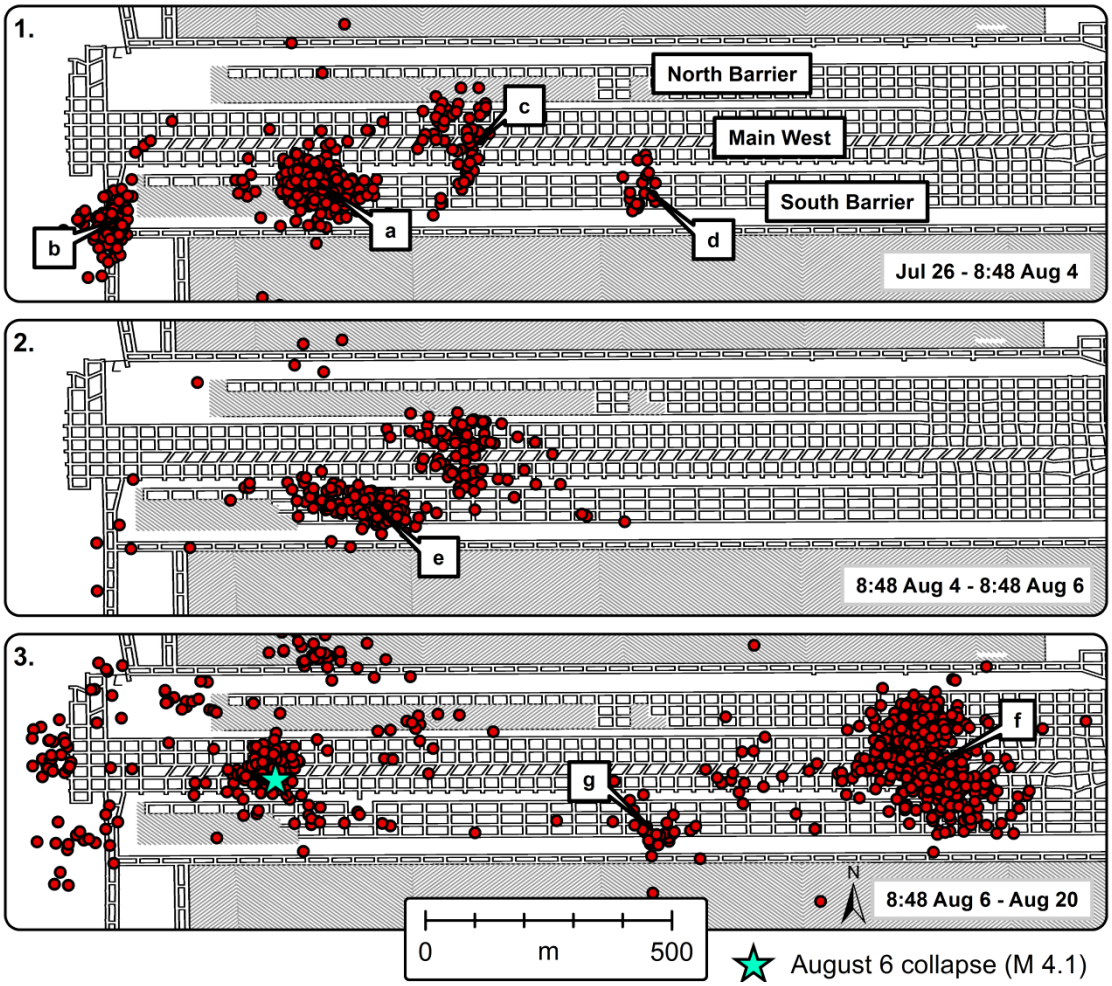

Figure 4.1. Double-difference locations of detected events presented in three panels

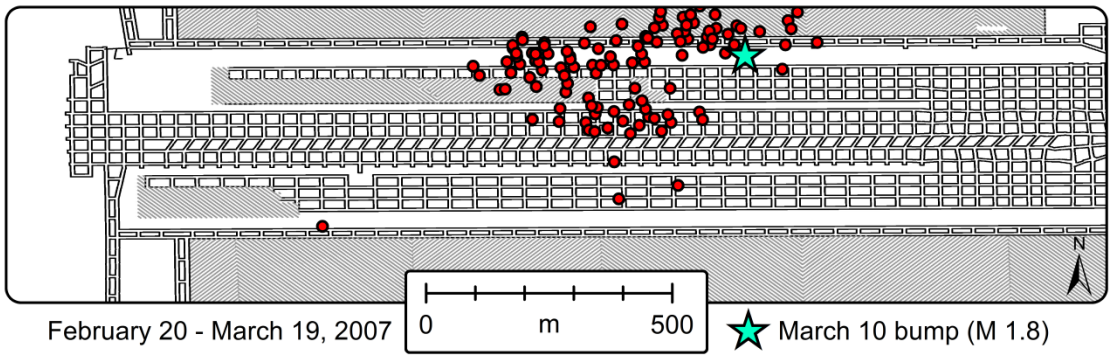

Figure 4.2. Double-difference locations of detected events related to the March bump

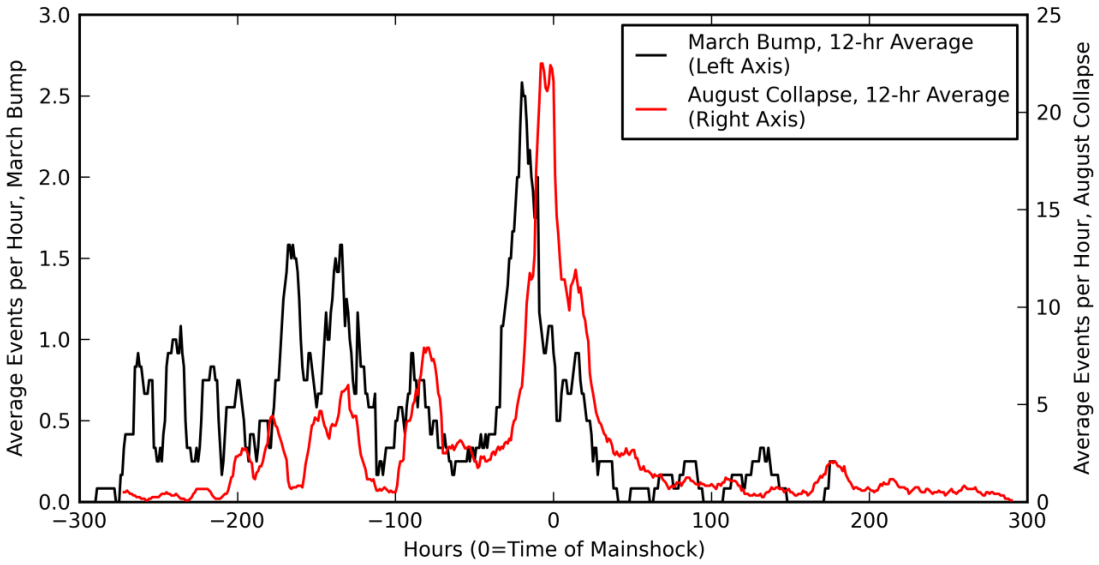

Figure 4.3. Average number of events per hour for March and August sequences

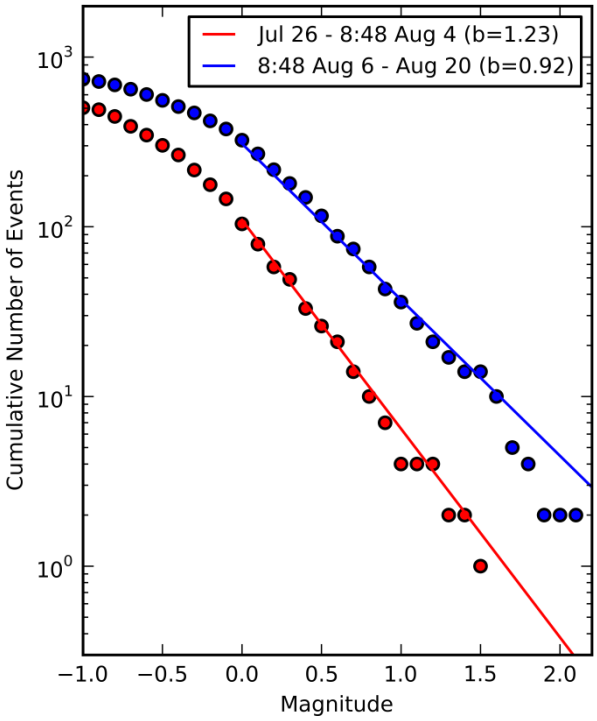

Figure 4.4. Frequency-magnitude plot comparing b-values precollapse and postcollapse

CHAPTER 5

CONCLUSIONS

This study demonstrates the potential for seismic monitoring to assist in improving mine safety in addition to improving understanding of mine collapse sequences and mechanics. Cross-correlation detection is a useful tool for monitoring MIS, especially when coupled with double-difference relocation techniques. Although cross-correlation detection is more computationally intensive than standard processing techniques, it allows for analysis of microseismicity on a level that could only be achieved previously through the use of dense, in-mine arrays. The techniques described here use only regional seismometers at distances of 20 to 30 km from the mine to detect and locate events (the temporary close-in stations were used only for detection-verification purposes where possible). A total of 1,494 seismic events were found to have occurred in close proximity to the main CCM collapse area between July 26 and August 19, 2007. Many of these events are as small as M –1.0 and are near or below the signal-to-noise ratio. Thus, they would likely be impossible to detect and locate using conventional short-term average/long-term average algorithms. The techniques applied here exhibit a 1.6 magnitude unit decrease in catalog completeness compared to conventional detection techniques.

The catalog of newly-detected events, when compared to the progression of mining, offers insight into the relationship between mining activity and collapse

mechanics in the case of CCM. Although much of the detected seismicity occurs in close proximity to the mining activity prior to the collapse, a significant amount is clustered along vertical joints throughout the area. As pillar-extraction approaches these seismically active joints, patterns in seismicity can be seen to shift. Furthermore, rates in seismicity can be seen to increase, and b-values can be seen to decrease. These factors do not necessarily indicate an impending collapse as varying levels of seismicity commonly occur in stable coal mines as well. It is difficult to conclude from a single case study whether this collapse could have been predicted. Nevertheless the results of this study show that cross-correlation detection of MIS with data from surface sensors may be useful in near-real time monitoring of mines and in evaluating the potential for mine collapse. With further study of MIS under different geologic conditions, it may be possible to identify areas of mines prone to dangerous levels of seismic activity.

Following the CCM collapse, patterns in seismicity can be seen to shift to the east of Main West and b-values decrease drastically. The events cluster in a shallow-dipping planar structure, suggesting lateral movement of bedding. Evidence of such movement was noted in logbook reports. The rate of these aftershocks was found to decay 28% faster than natural aftershock sequences observed throughout Utah. Knowledge regarding shifting locations and rates of postcollapse seismicity could eventually help rescue workers avoid dangerous areas, should collapses similar to that of the CCM occur in the future. A 25.2% decrease in b-value between events detected well before the collapse and well after the collapse suggests a noteworthy change in stress fields.

The detections reported here were made with extremely high confidence using a conservative *cc* threshold of 0.5. Although lowering this threshold increases the number

of detections, it decreases the quality of the locations and does not provide much new information regarding the nature of the collapse. Further research may be required regarding statistical arguments for the selection of *cc* thresholds as it is difficult to model the true probability of false detections. Improved precision in event locations can be achieved through data-interpolation as a way of increasing sampling rates. In this case study, it was unnecessary to interpolate beyond a sampling rate of 1 kHz (i.e., a factor of 10 smaller than the nominal sampling rate).

REFERENCES

Amitrano, D., Grasso, J.R., and Senfaute, G. 2005. Seismic precursory pattern before a cliff collapse and critical-point phenomena. *Geophys. Res. Lett.* 32:L08314. Accessed February 2014. doi:10.1029/2004GL022270.

Arabasz, W.J., and Hill, S.J. 1994. Aftershock temporal behavior and earthquake clustering in the Utah region. *Seismological Res. Lett.* 65(1):32.

Arabasz, W.J., Nava, S.J, and Phelps, W.T. 1997. Mining seismicity in the Wasatch Plateau and Book Cliffs coal mining districts, Utah, USA. In *Rockbursts and Seismicity in Mines*. Edited by S. J. Gibowicz and S. Lasocki. Rotterdam: A. A. Balkema.

Arabasz, W.J., and Pechmann, J.C. 2001. *Seismic characterization of coal-mining seismicity in Utah for CTBT monitoring.* Internal Report UCRL-CR-143772. Livermore, CA: Lawrence Livermore National Laboratory.

Boltz, M.S., Pankow, K.L., and McCarter, M.K. 2014. Fine details of mining-induced seismicity at the Trail Mountain coal mine using modified hypocentral relocation techniques. *Bull. Seismological Soc. Am.* (forthcoming). Accessed February 2014. doi: 10.1785/0120130011.

Burlacu, R., Roberson, P.M., Hale, J.M., Arabasz, W.J., Pechmann, J.C., and Pankow, K.L. 2007. *Earthquake Activity in the Utah Region: Preliminary Epicenters July 1 - September 30, 2007*. Quarterly Report. Salt Lake City, UT: University of Utah Seismograph Stations. www.quake.utah.edu/EQCENTER/QUARTERLY/REPORTS/2007/2007Q3_summ.pdf. Accessed February 2014.

Cheng, X., Niu, F., Silver, P.G., and Nadeau, R.M. 2011. Seismic imaging of scatterer migration associated with the 2004 Parkfield earthquake using waveform data of repeating earthquakes and active sources. *Bull. Seismological Soc. Am.* 101(3):1291–1301. Accessed February 2014. doi:10.1785/0120100261.

Doelling, H.H. 1972. *Central Utah coal fields: Sevier-Sanpete, Wasatch Plateau, Book Cliffs and Emery*. Utah Geological and Mineralogical Survey, Monograph Series, 3. Salt Lake City, UT: Utah Geological and Mineralogical Survey.

Dreger, D.S., Ford, S.R., and Walter, W.R. 2008. Source analysis of the Crandall Canyon, Utah, mine collapse. *Sci*. 321(5886):217. Accessed February 2014. doi:10.1126/science.1157392.

Ford, S.R., Dreger, D.S., and Walter, W.R. 2008. Source characterization of the 6 August 2007 Crandall Canyon mine seismic event in central Utah. *Seismological Res. Lett.* 79(5):637–644.

Gibbons, S.J., and Ringdal, F. 2006. The detection of low magnitude seismic events using array-based waveform correlation. *Geophys. J. Int*. 165:149–166. Accessed February 2014. doi:10.1111/j.1365-246X.2006.02865.x.

Gibowicz, S.J. 2009. Seismicity induced by mining: Recent research. *Adv. in Geophys.* 51:1–53.

Harris, D. 2006. *Subspace detectors: Theory*. Internal Report UCRL-TR-222758. Livermore, CA: Lawrence Livermore National Laboratory.

Harris, D., and Paik, T. 2006. *Subspace detectors: Efficient implementation.* Internal Report UCRL-TR- 223177. Livermore, CA: Lawrence Livermore National Laboratory.

Hasegawa, H.S., Wetmiller, R.J., and Gendziwill, D.J. 1989. Induced seismicity in mines in Canada—An overview. *Pageoph.* 129:423–453.

Hauksson, E., and Shearer, P. 2005. Southern California hypocenter relocation with waveform cross-correlation, Part 1: Results using the double-difference method. *Bull. Seismological Soc. Am.* 95(3):896–903. Accessed February 2014. doi:10.1785/0120040167.

Hayes, G.P., Bergman, E., Johnson, K.L., Benz, H.M., Brown, L., and Meltzer, A.S. 2013. Seismotectonic framework of the 2010 February M_w 8.8 Maule, Chile earthquake sequence. *Geophys. J. Inter.* 195:1034–1051. Accessed February 2014. doi:10.1093/gji/ggt238.

Ide, S., Baltay, A., and Beroza, G.C. 2011. Shallow dynamic overshoot and energetic deep rupture in the 2011 M_w 9.0 Tohoku-Oki earthquake. *Sci.* 332:1426–1429. Accessed February 2014. doi:10.1126/science.1207020.

Kubacki, T.M., McCarter, M.K., and Pankow, K.L. 2012. Post-collapse seismicity of the Crandall Canyon Mine using double difference relocations. *31st Int. Conf. on Ground Control in Min*. 31:217–221.

Lu, Z., and Wicks, C. 2010. Characterizing 6 August 2007 Crandall Canyon mine collapse from ALOS PALSAR InSAR. *Geomatics, Nat. Hazards and Risk*. 1(1):85–93.

MacQueen, J.B. 1967. Some methods for classification and analysis of multivariate observations. *5th Berkeley Symposium Math. Stat. Probab*. 5(1):281–297.

Maleki Technologies, Inc. 2005. *Control of Mining-Induced Seismicity through Mine Design Application of U.S. Experience and Numeric Modeling the Cottonwood Tract*. Technical progress report. Spokane, WA: School and Institutional Trust Lands Administration.

Michelini, A., and Bolt, B.A. 1986. Application of the principal parameters method to the 1983 Coalinga, California, aftershock sequence. *Bull. Seismological Soc. Am. 76*(2):409–420.

MSHA (Mine Safety and Health Administration). *2007. Coal Mine Safety and Health Report of Investigation, Underground Coal Mine, Fatal Underground Coal Burst Accidents August 6 and 16, 2007, Crandall Canyon Mine, Genwal Resources, Inc.* Report. Arlington, Virginia: MSHA.

Pankow, K.L., McCarter, M.K., Arabasz, W.J., and Burlacu, R.L. 2008. Coal-mining-induced seismicity in Utah—Improving spatial resolution using double-difference relocations. *27th Int. Conf. on Ground Control in Min.* 27:91–97.

Pechmann, J.C., Arabasz, W.J., Pankow, K.L., Burlacu, R., and McCarter, M.K. 2008. Seismological report on the 6 August 2007 Crandall Canyon mine collapse in Utah, *Seismological Res. Lett.* 79(5):620–636.

Phillips, W.S., Pearson, D.C., Yang, X., and Stump, B.W. 1999. Aftershocks of an explosively induced mine collapse at White Pine, Michigan. *Bull. Seismological Soc. Am*. 89(6):1575–1590.

Plattner, C., Wdowinski, S., Dixon, T.H., and Biggs, J. 2010. Surface subsidence induced by the Crandall Canyon Mine collapse: InSAR observations and elasto-plastic modeling. *Geophy. J. Int.* 183(3):1089–1096.

Rowe, C.A., Stead, R.J., Begnaud, M.L., and Morton, E.A. 2012. Seismic signal analysis for event detection and categorization. *2012 Monitoring Research Review: Ground-Based Nuclear Explosion Monitoring Technologies*. pp. 312–320.

Rubin, A.M., Gillard, D., and Got, J.L. 1999. Streaks of microearthquakes along creeping faults. *Nat.* 400(6745):635–641.

Schaff, D.P., Bokelmann, G.H.R., Ellsworth, W.L., Zanzerkia, E., Waldhauser, F., and Beroza, G.C. 2004. Optimizing correlation techniques for improved earthquake location. *Bull. Seismological Soc. Am.* 94(2):705–721.

Schaff, D.P., and Waldhauser, F. 2005. Waveform cross-correlation-based differential travel-time measurements at the Northern California Seismic Network. *Bull. Seismological Soc. Am.* 95(6):2446–2461.

Schaff, D. 2010. Improvements to detection capability by cross-correlation for similar events: a case study of the 1999 Xiuyan, China, sequence and synthetic sensitivity tests. *Geophys. J. Int.* 180(2):829–846.

Shearer, P.M. 1997. Improving local earthquake locations using the L1 norm and waveform cross-correlation: Application to the Whittier Narrows, California, aftershock sequence. *J. Geophys. Res.* 102(B4):8269.

Spottiswoode, S.M., and Milev, A.M. 1998. The use of waveform similarity to define planes of mining-induced seismic events. *Tectonophysics.* 289:51–60.

Trifu, C.I., and Shumila, C. 2010. Microseismic monitoring of a controlled collapse in Field II at Ocnele Mari, Romania. *Pageoph.* 167:27–42.

Utsu, T. 1961. A statistical study on the occurrence of aftershocks. *Geophys. Mag.* 30:521–605.

Vallejos, J.A. and McKinnon, S.D. 2010. Omori's law applied to mining-induced seismicity and re-entry protocol development. *Pageoph.* 167:91–106.

VanDecar, J.C. and Crosson, R.S. 1990. Determination of teleseismic relative phase arrival times using multi-channel cross-correlation and least squares. *Bull. Seismological Soc. Am.* 80(1):150–169.

Waldhauser, F., and Ellsworth, W.L. 2000. A double-difference earthquake location algorithm: Method and application to the northern Hayward fault, California. *Bull. Seismological Soc. Am.* 90(6):1353–1368.

Waldhauser, F., and Schaff, D.P. 2008. Large-scale relocation of two decades of Northern California seismicity using cross-correlation and double-difference methods. *J. Geophys. Res.* 113(B8). Accessed February 2014. doi:10.1029/2007JB005479.

Whidden, K.M., and Pankow, K.L. 2012. A catalog of regional moment tensors in Utah from 1998 to 2011. *Seismological Res. Lett.* 83(5):775–783. Accessed February 2014. doi:10.1785/0220120046.

Wiemer, S. 2001. A software package to analyze seismicity—ZMAP. *Seismological Res. Lett. 72*(3):373–382.

Wiggins, R.A. 1976. Interpolation of digitized curves. *Bull. Seismological Soc. Am.* 66(6):2077–2081.

Yang, H., Zhu, L., and Chu, R. 2009. Fault-plane determination of the 18 April 2008 Mount Carmel, Illinois, earthquake by detecting and relocating aftershocks. *Bull. Seismological Soc. Am.* 99(6):3413–3420.